[10]A. Abrikosov, L. Gorkov, and I. Dzyaloshinskii, *Methods of Quantum Field Theory in Statistical Physics* (Prentice-Hall, Englewood Cliffs, N.J., 1963), pp. 139–143; G. Eliashberg, Zh. Eksperim. i Teor. Fiz. 43, 1005 (1962) [Soviet Phys. JETP 16, 780 (1963)].

[11]For the possibility of coupling between spin and density fluctuations, see for example, W. Brinkman and S. Engelsberg, Phys. Rev. 169, 417 (1968), p. 430.

[12]One may at this stage note that this relation is quite different from the one used by Fowler and Prange (Ref. 2) [the integral of their Eq. (24) with respect to $E_F$]. Their equation corresponds to using $\Omega_{el} = (1/\beta) \Sigma_n \text{tr} \times \{\ln[-G^{-1}(\omega_n)]\}$. By following the arguments of Luttinger, we will show that their result is correct if one considers only the oscillatory part of the thermodynamic potential.

[13]W. McMillan, Phys. Rev. 167, 331 (1967).

[14]C. Herring, in *Magnetism*, Vol. IV, edited by G. Rado and H. Suhl (Academic, New York, 1966), pp. 294–296.

[15]E. Titchmarsh, *Introduction to the Theory of Fourier Integrals* (Oxford U.P., London, 1948), Sec. 2.8.

[16]J. R. Schrieffer, *Theory of Superconductivity* (Benjamin, New York, 1964).

[17]D. Amit, J. Kane, and H. Wagner, Phys. Rev. Letters 19, 425 (1967); Phys. Rev. 175, 313 (1968); 175, 326 (1968).

[18]R. R. Oder, Bull. Am. Phys. Soc. 14, 321 (1969).

[19]E. Bucher, W. Brinkman, J. Marta, and H. Williams, Phys. Rev. Letters 18, 1125 (1967).

[20]This has been confirmed experimentally by D. Schoenberg and J. Vanderkooy, J. Low Temp. Phys. (to be published).

# Low-Energy Electron Diffraction from Liquid Hg:
## Multiple Scattering, Scattering Factor, and Attenuation*

J. S. Schilling[†] and Maurice B. Webb

*University of Wisconsin, Madison, Wisconsin* 53706

(Received 2 March 1970)

The elastic scattering of electrons from liquid Hg has been measured for energies between 100 and 500 eV and for scattering angles between 60° and 170°. The observed scattering is remarkably similar to that from Hg vapor; a model calculation shows that the differences between the liquid and vapor scattering are due to multiple scattering and inelastic processes. The analysis shows that (i) higher-order multiple scatterings are strongly attenuated by inelastic processes; (ii) approximately half the observed integrated intensity has been scattered only once; (iii) for back angles, the atomic scattering factor is essentially the same for the atoms in the liquid and the vapor; and (iv) attenuation coefficients for elastic electrons are of the order of several tenths of a reciprocal angstrom.

## I. INTRODUCTION

The difficulties in developing a satisfactory understanding of low-energy electron diffraction are well known and arise because of the strong interactions between the electron and the crystal.[1] Because of the large elastic cross section, multiple scattering must be important, and most current theoretical work aims to develop dynamic theories in which either band-structure calculations are extended to the energies of the incident electron[2] or, equivalently, in which the multiple scattering is treated explicitly in a self-consistent way.[3] In these theoretical treatments one needs either the lattice potential or the related atomic scattering factor, neither of which has generally been available from experiment. The inelastic interactions are also strong and have an important effect on the elastic scattering. They have been included in some recent calculations,[1,4] usually in a phenomenological way. Little experimental information is available about the attenuation of the elastic beams due to inelastic processes.

It is the purpose of this paper to report the results and interpretation of experiments on the low-energy electron scattering from liquid Hg. These experiments allow reasonably direct estimates of the multiple-scattering contribution, of the inelastic absorption coefficient, and of the atomic scattering factor.

An earlier paper[5] reported a generally applicable method to measure what was called the square of the effective atomic scattering factor, $|f(\theta, E)|^2_{eff}$. In that work the elastic scattering of low-energy electrons from the surface of a Ni crystal at elevated temperatures was measured as a function of the scattering angle $2\theta$ for various angles of incidence. The observed scattered intensity could be divided into two parts, one part which depended on the crystal structure and its orientation and a second part which did not. This latter part, which is dominant at high temperatures, gives the angular dependence of $|f(\theta, E)|^2_{eff}$. After correction

for absorption this would be the angular dependence of the true $|f(\theta,E)|^2$ except for multiple-scattering contributions. It was suggested in that work that an indication of the upper limit to the multiple scattering is given by minima in $|f(\theta,E)|^2_{eff}$, since the higher-order scatterings will have a relatively flat angular dependence. Since the minima were quite deep, it was estimated that the multiple-scattering contributions were small. As will be seen, the present experiments on liquid Hg are similar to the Ni work, since, for the momentum transfer used, the interference function is essentially constant and the scattering is nearly independent of the short-range order in the liquid. Unlike for Ni, however, experimental data are available[6] for the electron scattering from Hg vapor, and they show considerable structure in the angular dependence of the elastic scattering. This prior knowledge will be important in the interpretation of the scattering from the liquid.

Our experiments are closely related to those of Eitel, Jost, and Kessler,[6] who measured the angular distribution and polarization of electrons elastically scattered from Hg vapor as a function of vapor density and attributed observed changes to multiple scattering. Also, Eckstein[7] has measured the scattering and polarization by Hg condensed and frozen on a substrate. His results are similar to ours where they can be compared. He also mentions multiple scattering as one possible explanation of the observed differences between the scattering from the condensed phase and the vapor. Jordan and Brode[8] made measurements of the scattering of 20–70-eV electrons from liquid Hg and noticed a peak in the scattering in the backward direction.

## II. EXPERIMENTAL

The apparatus is shown schematically in Fig. 1. A standard volume of liquid Hg from a continuously operating still can be transferred to a sample cup in the center of the scattering chamber. In the cup the sample forms a drop 2. 5 cm in diameter so that the curvature of the surface at the center is negligible. The drop can be removed from the cup by adding extra Hg until the whole drop runs out an opening in the side of the cup and returns to the still. The sample temperature is controlled either by conduction through a Cu rod in contact with the bottom of the cup or by flowing cold gas up the tube supporting the cup.

Two electron guns provide beams with grazing angles of incidence of 81° and 59. 5°. Incident beams have a diameter of less than 1 mm at the sample and a divergence of less than 1°.

The elastically scattered electrons are detected in a Faraday cage which rotates about an axis in
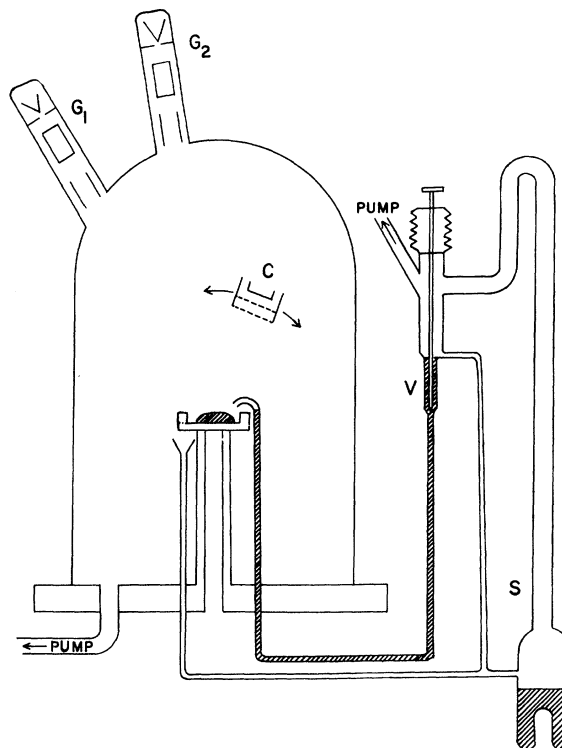


FIG. 1. Schematic drawing of apparatus. $G_1$, $G_2$: electron guns; S: Hg still; V: needle valve; C: collector rotating about horizontal axis normal to the figure and in the plane of the sample drop.

the plane of the sample surface normal to the plane of incidence. The width of the Faraday cage prevented measurements closer than 10° to the backward direction. The aperture of the Faraday cage is a rectangular slit 1×3 mm, 3 cm from the axis of rotation. A fine grid over the aperture reduces fringing fields; the retarding potential is applied to a second grid to select only elastically scattered electrons; and finally a plate, whose potential is near that of the crystal, collects the electrons. This arrangement prevents positive ions produced in the Hg vapor by the incident beam from reaching the collector or its leads. Without this precaution there is a positive background current proportional to the Hg vapor pressure. The energy resolution of the detector was limited by the geometry of the retarding field and was 4% of the incident energy.

The entire system was baked out and pumped to a pressure of $10^{-10}$ Torr. Then Hg with a specified impurity content of less than one part in $10^9$ was introduced into the still under vacuum.[9] The still was operated continuously.

The scattered intensity could be measured within 15 sec after introducing a fresh drop to the sam-

ple cup and was observed to be constant for at least the next 15 min, which is the time necessary to complete a measurement of the angular dependence of the scattering. A bulk impurity concentration as large as one part in $10^7$ is required so that if all the impurity atoms were adsorbed on the surface they would form a monolayer. Assuming a diffusion coefficient for the impurity equal to the known self-diffusion coefficient of Hg, this adsorption would require approximately 1 h. Partial pressure of adsorbable gases of the order of $10^{-7}$ Torr would be required in order to adsorb an appreciable part of a monolayer of impurities within 15 sec. From these estimates it seems reasonable that the data are unaffected by impurities on the Hg surface.

The angular dependence of the elastically scattered intensity was measured for 12 energies between 80 and 500 eV for each of two angles of incidence. Examples of the data are shown in Figs. 2 and 3. The dashed lines are the corresponding
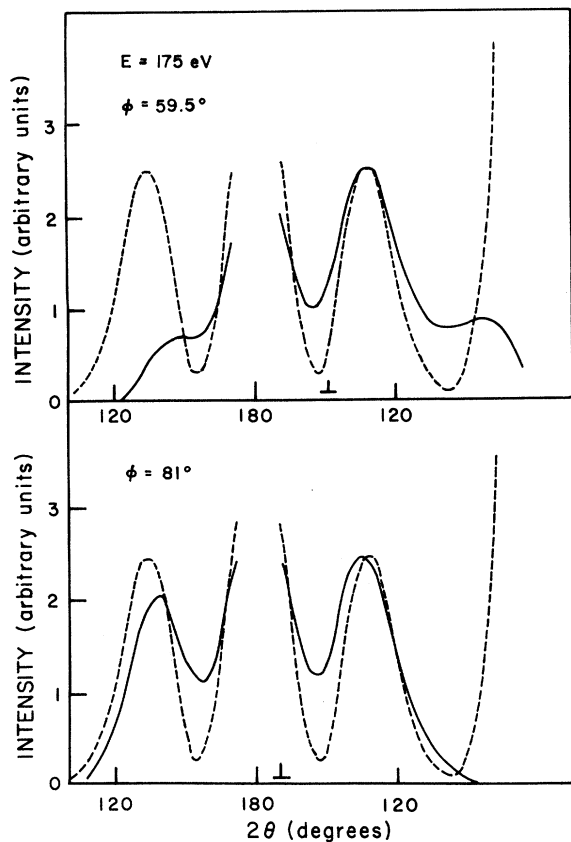


FIG. 2. Scattered intensity versus scattering angle at an energy of 500 eV. The solid curve is the measured intensity from the liquid. ⊥ indicates the surface normal. The dashed line is the scattering from Hg vapor from Ref. 11.
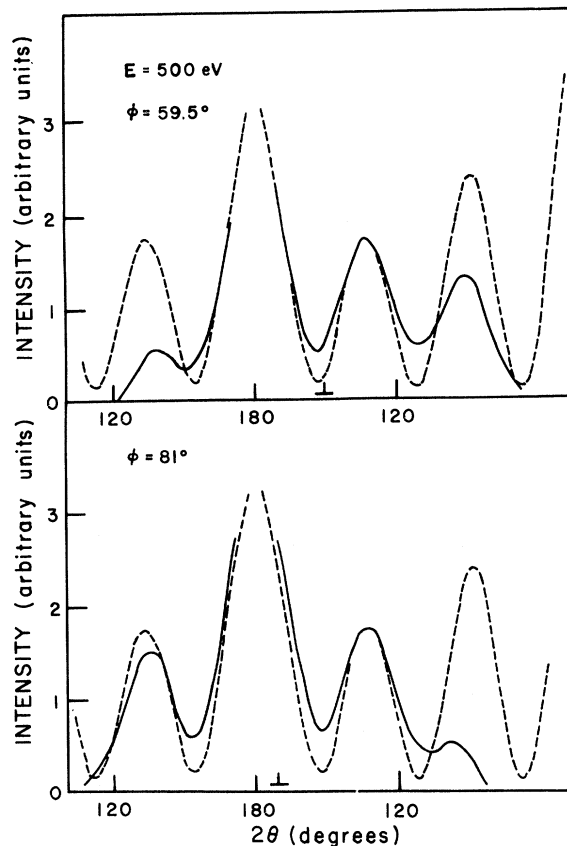


FIG. 3. Scattered intensity versus scattering angle at an energy of 175 eV. The solid curve is the measured intensity from the liquid. ⊥ indicates the surface normal. The dashed line is the scattering from Hg vapor from Ref. 10.

results for the scattering from Hg vapor.[10,11] Other data are plotted as the solid lines in Figs. 7 and 8, where the results are compared with the analysis.

The most striking result is the similarity of the scattering from the liquid and the vapor. In all the data except for those where scattered beams make small grazing angles with the surface, the positions of the peaks and their relative magnitudes are nearly the same as for the scattering from free atoms. This strongly suggests without detailed analysis that at back angles the atomic scattering factor is essentially the same as for the free atom and that single-scattering events make a major contribution to the scattering.

There are two apparent differences between the liquid and gas results. First, the scattering from the liquid is weaker when the scattered beam makes small angles with respect to the surface. This attenuation is expected because of inelastic processes and will be dealt with in detail in Sec. III.

The second difference is that the minima in the angular dependence of the scattering from the liquid are relatively less deep than for the vapor. Although one might think of several possible explanations of this feature, here we will consider the effect of multiple scattering. One expects considerable multiple scattering because the atomic total elastic cross section is near geometrical; further, the multiple scattering will tend to fill the valleys because it will have a more uniform angular distribution than the single scattering. That this is the major cause of the difference between the scattering from the vapor and the liquid is demonstrated by the success of the analysis to follow.

### III. MODEL CALCULATION

The relative importance of the single-and multiple-scattering contributions will depend on the relative importance of the elastic and inelastic processes. To illustrate this we first make a plausibility argument and then give a model calculation.

Suppose that atoms scatter isotropically with a total elastic cross section $\sigma_{el}$ and that in the liquid there is sufficient disorder so that it is appropriate to add intensities rather than amplitudes. Suppose further that the elastic beam is attenuated according to an attenuation coefficient $\mu_t$ due to both elastic and inelastic processes. Then the contribution to the observed intensity from those electrons which have been scattered only once will be proportional to $\rho\sigma_{el}/\mu_t$. Here $\rho$ is the number density of atoms. Neglecting angular factors and details of path lengths, the functional dependence of the twice-scattered contribution on $\sigma_{el}$ and $\mu_t$ is given by considering the once-scattered electrons to be the incident beam for the second scattering. Thus this intensity is proportional to $(\rho\sigma_{el}/\mu_t)^2$ and so forth for higher orders. Each successive order is reduced by an additional factor $\rho\sigma_{el}/\mu_t$. Physically this expresses the fact that for an electron to be elastically scattered several times it must travel farther through the crystal and therefore will be more strongly attenuated. Since for low-energy electrons $\sigma_{el}$ and $\sigma_{in}$ are comparable, $\rho\sigma_{el}/\mu_t$ is of the order of $\frac{1}{2}$, the series of contributions from successive orders converges rapidly, and the contribution from once-scattered electrons is dominant.

We now wish to make this qualitative argument more precise and calculate an approximate expression for the elastic backscattering of electrons from a liquid. It is assumed that the elastic scattering is described by an atomic scattering factor $f(\theta, E)$ appropriate to an atom in the liquid and that it is sufficient to use the asymptotic form of $f(\theta, E)$ to calculate the multiple scattering. Second, it is assumed that the attenuation of a beam of elastic

electrons moving through the bulk is described by a linear attenuation coefficient $\mu_t$ which is independent of both the direction of the beam and the depth in the liquid. (This implies the further assumption that the surface losses take place either at or outside the surface. These losses will be accounted for later.) We define $\mu_t = \mu_{in} + \rho\sigma_{el}$, where $\mu_{in}$ is due to inelastic processes and $\sigma_{el}$ is the total elastic cross section. Finally, it is assumed that the pair distribution function is independent of the interatomic separation and thus the interference function is constant independent of the diffraction vector $\vec{S} = \vec{k} - \vec{k}_0$. We thus may neglect interference between atoms and add intensities instead of amplitudes.

This last assumption requires additional comment. For the data presented here, $|\vec{S}| > 5 \, Å^{-1}$, corresponds to the third halo and beyond in the interference function of bulk Hg known from x-ray experiments[12]; here variations in the interference function are less than 10%. This assumption is also consistent with the experimental results for the diffraction of low-energy electrons from a Ni crystal at high temperatures where the major part of the scattering is independent of the crystal and its orientation.[5] However, this approximation is not good for small $|\vec{S}|$, or forward scattering, which enters our calculation of the multiple-scattering contributions through convolution integrals. Fortunately, as will be seen, the results are rather insensitive to the detailed shape of the multiple scattering; the effect of the uncertainty in the forward scattering will be discussed later when we compare the result of the model calculation with the data.

Under these assumptions the intensity per unit incident intensity and per unit solid angle of electrons which have been elastically scattered once and only once is

$$I_1(\vec{S}) = A \int_0^\infty \exp\left(-\frac{\mu_t z_1}{\sin\phi}\right) \frac{\rho dz_1}{\sin\phi} \, |f(\theta, E)|^2 \, \exp\left(\frac{-\mu_t z_1}{\sin\phi'}\right)$$

$$= \frac{A\rho |f(\theta, E)|^2}{\mu_t (1 + \sin\phi/\sin\phi')} , \quad (1)$$

where $\phi$ and $\phi'$ are the grazing angles of the incident and scattered beams, respectively, $A$ is the cross-sectional area of the incident beam, and $Adz_1/\sin\phi$ is the element of scattering volume. This is the absorption correction familiar in x-ray reflection experiments from mosaic crystals.

Similarly the intensity of twice-scattered electrons is given by

$$I_2(\vec{S}) = A \int_0^\infty \exp\left(\frac{-\mu_t z_1}{\sin\phi}\right) \int_{4\pi} \frac{\rho dz_1}{\sin\phi} \, |f(\theta_1, E)|^2 d\Omega_1$$

$$\times \int_{z_{min}}^{z_{max}} \exp\left(\frac{-\mu_t |z_2 - z_1|}{\cos\gamma}\right) \frac{\rho dz_2}{|\cos\gamma|}$$

$$\times |f(\theta_2, E)|^2 \exp\left(\frac{-\mu_t z_2}{\sin\phi'}\right) . \qquad (2)$$

Here the first and second scatterings take place in elements of depth $dz_1$ and $dz_2$ at $z_1$ and $z_2$; $\theta_2$ is fixed by $\vec{S}$, the azimuth of the first scattering, and $\theta_1$; and $\gamma$ is the angle between the once-scattered beam and the $z$ axis. The limits of integration over $z_2$ depend on whether the first scattering is toward or away from the surface. The factor $\exp(-\mu_t \times |z_2 - z_1|/\cos\gamma)$ is the attenuation between the first and second scatterings.

Since $|f(\theta, E)|^2$ is strongly peaked in the forward direction, the important contributions to the integrals arise when one or the other scattering is in nearly the forward direction. Thus $|\cos\gamma| \approx \sin\phi$ if the first scattering is away from the surface and $\approx \sin\phi'$ if the first scattering is toward the surface. With this approximation

$$I_2(\vec{S}) = \frac{A\rho^2}{2\mu_t^2(1+\sin\phi/\sin\phi')} \int |f(\theta_1, E)|^2 |f(\theta_2, E)|^2 d\Omega_1 . \qquad (3)$$

A similar calculation of the triple scattering with analogous approximations gives

$$I_3(\vec{S}) = \frac{A\rho^3}{3\mu_t^3(1+\sin\phi/\sin\phi')} \int\int |f(\theta_1, E)|^2$$

$$\times |f(\theta_2, E)|^2 |f(\theta_3, E)|^2 d\Omega_1 d\Omega_2. \qquad (4)$$

The total scattering is

$$I_T(\vec{S}) = \frac{A}{(1+\sin\phi/\sin\phi')} \left( \frac{\rho|f(\theta, E)|^2}{\mu_t} + \frac{\rho^2}{2\mu_t^2} \int |f(\theta_1, E)|^2 \right.$$

$$\times |f(\theta_2, E)|^2 d\Omega_1 + \frac{\rho^3}{3\mu_t^3} \int\int |f(\theta_1, E)|^2$$

$$\left. \times |f(\theta_2, E)|^2 |f(\theta_3, E)|^2 d\Omega_1 d\Omega_2 + \cdots \right)$$

$$= \frac{A}{(1+\sin\phi/\sin\phi')} [I_1'(\vec{S}) + I_2'(\vec{S}) + I_3'(\vec{S}) + \cdots ] . \qquad (5)$$

Before this series can be compared to the experimental data, we must consider the additional attenuation due to the inelastic "surface losses" first discussed by Ritchie.[12] Assuming these losses occur at or outside the surface of the liquid, their only effect is to attenuate the elastic beams an amount depending on their energy and direction with respect to the surface. The differential probability that an electron loses energy $\Delta E$ and is scattered through an angle $\theta$ into a solid angle $d\Omega$ while crossing the surface of the liquid is[13]

$$\frac{d^2p}{d(\Delta E)d\Omega} = \frac{1}{2\pi^2 a_0 kE} \frac{\theta}{(\theta^2 + \theta_E^2)^2} \left[ \frac{1+\theta_E^2/\theta^2}{\sin^2\phi} \right.$$

$$\left. - \left(\cot\phi \, \cos\psi + \frac{\theta_E}{\theta}\right)^2 \right]^{1/2} \text{Im}\left(\frac{(1-\epsilon^2)}{\epsilon(\epsilon+1)}\right), \qquad (6)$$

where $a_0$ is the Bohr radius, $\theta_E = \Delta E/2E$, $\phi$ is the grazing angle of incidence, $\psi$ is the azimuthal angle

of scattering measured from the plane of incidence, and $\epsilon$ is the complex dielectric constant. This expression was integrated numerically over all solid angle and energy loss to $\Delta E = 20$ eV using $\epsilon$ for liquid Hg from the data of Wilson and Rice.[14] This gives the total probability that an electron crossing a surface suffers an energy loss:

$$p(\phi) = 2.76/E^{1/2} \sin\phi, \qquad (7)$$

where $E$ is in eV. The elastic scattering of Eq. (5) must be multiplied by the factor $1-p(\phi)$ for the incident beam and by $1-p(\phi')$ for the scattered beam. This can only be correct for sufficiently large values of $\phi$, where $p(\phi) \ll 1$. We know of no more satisfactory calculation of $p(\phi)$ for small $\phi$ and we should not expect this model calculation to compare well with experiment for small grazing angles.

## IV. COMPARISON OF MODEL WITH DATA

We now compare the results of this model calculation with the experimental data.

One feature which can be checked immediately without knowing the values of any of the parameters or adding further assumptions is the dependence of the observed scattering on the grazing angles of incidence and scattering, $\phi$ and $\phi'$. This entire dependence is contained in the factors

$$\left(1 - \frac{2.76}{E^{1/2}\sin\phi}\right)\left(1 - \frac{2.76}{E^{1/2}\sin\phi'}\right)\frac{1}{(1+\sin\phi/\sin\phi')} .$$

In Fig. 4(a) we superimpose data taken on both sides of $2\theta = 180°$ for $\phi = 59\frac{1}{2}°$ and $E = 522$ eV. In Fig. 4(b) we replot the same data after division by the above three factors. It is apparent that the asymmetry in the data is accounted for by the model calculation for $\phi \gtrsim 10°$. For smaller $\phi'$ the analysis leading to Eq. (7) fails.

We now want to compare the angular dependence of the elastic scattering expected from the model calculation with the experimental results. This requires the knowledge of the function $|f(\theta, E)|^2$ and of $\mu_t$. The strong similarity between the back scattering from the liquid and from the free atom suggests that for back angles we use the $|f(\theta, E)|^2$ from gas data. However, it is clear from the fact that the total elastic cross section of the free atom is approximately the geometrical cross section of an atom in the liquid that the forward scattering cannot be the same for a free atom and one in the liquid. The large forward peak in the gas scattering contains $\approx 70\%$ of the total elastic scattering. This peak, which is due mainly to peripheral collisions, will be changed considerably by putting an atom in the liquid where the outer regions of the atom are strongly perturbed and where the incident electron is screened by the conduction elec-
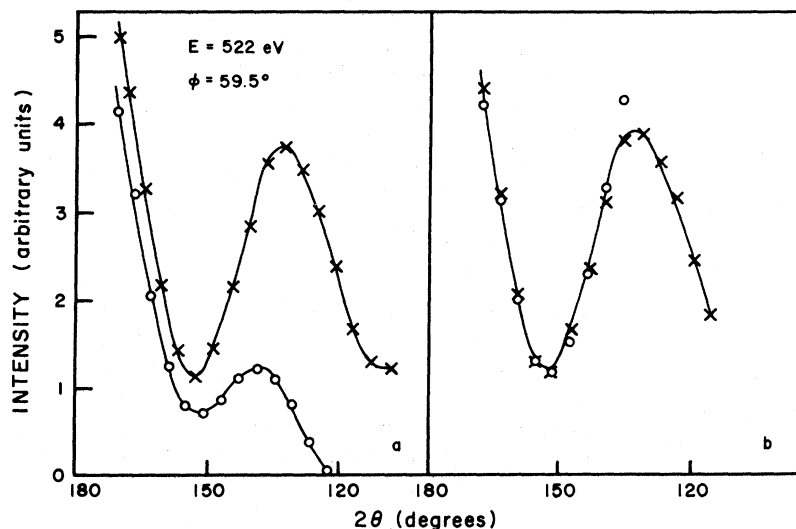
FIG. 4. Dependence of scattering on $\phi$ and $\phi'$. (a) Scattered intensity versus scattering angle for $E = 522$ eV and $\phi = 59.5°$. The data from either side of $2\theta = 180°$ are superimposed. (b) Same data as in (a) divided by the factors

$$\left(1 - \frac{2.76}{E^{1/2}\sin\phi}\right)\left(1 - \frac{2.76}{E^{1/2}\sin\phi'}\right)$$

$$\times \left(\frac{1}{1 + \sin\phi/\sin\phi'}\right) .$$

trons in distances like the Thomas-Fermi screening radius. One expects this peak to be both broader and smaller for an atom in the liquid. In addition, it is at the forward angles that errors due to the assumption that the interference function is constant are serious. Because of these uncertainties we cannot evaluate the convolutions in Eq. (5) accurately. However, we can make two approximations which will give, respectively, over- and underestimates of the multiple-scattering contributions.

In the first approximation, we ignore the difficulty just discussed and use the free-atom scattering factor for all $2\theta$. The only remaining parameter in Eq. (5) is $\mu_t$, and since $\sigma_{el}$ ha been assumed, it is only left to choose $\mu_{in}$. We will treat $\mu_{in}$ as an adjustable parameter, the choice of which in effect adds sufficient multiple scattering to fill the valleys in $I_1'(S)$ so the sum most nearly coincides with the experimentally observed scattering. In this first approximation, where we use an $|f(\theta, E)|^2$ which has too large and sharp a forward peak, convolutions for the multiple scattering will have exaggerated maxima and minima at the same angles as in the single scattering. Because of this exaggerated structure a larger relative contribution from these multiple-scattering terms is necessary than would be required if we used a more correct $|f(\theta, E)|^2$. In this sense this approximation overestimates the multiple-scattering contributions.

We now evaluate Eq. (5). For energies of 200 eV and greater we use $|f(\theta, E)|^2$ from Kessler's[11] gas data for $10° < 2\theta < 150°$ and from Holzwarth and Meister's[15] calculations to complete the angular range. For energies below 200 eV, $|f(\theta, E)|^2$ is from results of Jordan and Brode[8] and of Schon-

felder and Bunyan[10] for $10 < 2\theta < 170°$ and estimates for the remaining angles. For the second term, $I_2'(\vec{S})$, the convolution integral $\int |f(\theta_1, E)|^2 |f(\theta_2, E)|^2 \times d\Omega_1$ was evaluated numerically for the several energies between 100 and 500 eV; an example is shown in Fig. 5. As expected, the convolution is considerably flatter than $|f(\theta, E)|^2$; however, the positions of the peaks and valleys are the same.

To evaluate $I_3'(\vec{S})$ and higher-order convolutions would require a considerable computation. However, these terms will be both small and nearly uniform in $2\theta$, and their detailed evaluation does not seem warranted. Instead we make the following approximation. Recognizing that $|f(\theta, E)|^2$ is strongly peaked in the forward direction, the main contribution to the convolutions comes from multiple-scattering events in which all but one of the scatterings is near forward. Then we have

$$\int |f(\theta_1, E)|^2 |f(\theta_2, E)|^2 \cdots |f(\theta_n, E)|^2 d\Omega_1 \cdots d\Omega_{n-1}$$

$$\simeq n \langle |f(\theta, E)|^2 \rangle (\sigma_{el}^f)^{n-1}, \qquad (8)$$

where $\sigma_{el}^f$ is the cross section for scattering into the forward peak and where $\langle |f(\theta, E)|^2 \rangle$ is a weighted average taken over an angular range centered at $2\theta$. For $I_3'(\vec{S})$, $|f(\theta, E)|^2$ should be averaged over a range approximately equal to that of the forward peak; for higher-order scatterings this average is over successively broader ranges. For the third- and higher-order terms we replace $\langle |f(\theta, E)|^2 \rangle$ by its average over the entire back hemisphere denoted by $\sigma_{el}^b$. The third- and higher-order terms are now represented by a geometric series which may be summed, and finally,

$$I_T(\vec{S}) = \left(1 - \frac{2.76}{E^{1/2}\sin\phi}\right)\left(1 - \frac{2.76}{E^{1/2}\sin\phi'}\right)$$
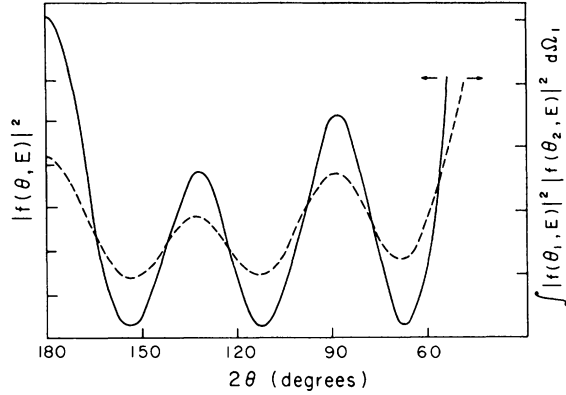
FIG. 5. Angular dependence of $|f(\theta,E)|^2$ and of $\int |f(\theta_1,E)|^2 |f(\theta_2,E)|^2 d\Omega_1$. The solid line is $|f(\theta,E)|^2$ from Ref. 11 and 15. The dashed curve is the convolution integral.

$$\left(\frac{1}{1+\sin\phi/\sin\phi'}\right)\left(\frac{\rho\,|f(\theta,E)|^2}{\mu_t}+\frac{\rho^2}{2\mu_t^2}\int |f(\theta_1,E)|^2\right.$$

$$\left.\times\,|f(\theta_2,E)|^2 d\Omega_1+\frac{\rho^2\sigma_{el}^{b}\sigma_{el}^{f}}{2\pi\mu_t^2\,(\mu_t/\rho\sigma_{el}^{f}-1)}\right);\qquad(9)$$

We now evaluate Eq. (9) using $\mu_t$ as an adjustable parameter. This has been done for three to five values of $\mu_t$ for each energy. In Fig. 6 we show the results for 500 eV and three values of $\mu_t$. These curves have been normalized to the experimental point at $2\theta = 132°$. It is seen that there is a value of $\mu_t$ which gives a surprisingly good fit to the experimental data for scattering angles such that $\phi' \gtrsim 15°$. For smaller values of $\phi'$ the surface-loss correction becomes progres-

sively less accurate and the calculated curves fall below the data. The effect of the attenuation is in accordance with the qualitative argument given above: A larger $\mu_t$ gives less multiple scattering and the calculated curves have deeper valleys and resemble more closely the single-scattering result and vice versa. From the figure it is clear that $\mu_t$'s about 20–30% different from the best value give noticeably poorer fits.

A comparison of the results of the model calculation with the data using the best values of $\mu_t$ at each energy is shown in Figs. 7 and 8. The dots are the result of this analysis and the solid lines are the experimental data. $\mu_t$ was chosen comparing the calculated curves with the data for $\phi = 81°$ and this same value then was used to calculate $I_T(\vec{S})$ for $\phi = 59.5°$. Over the energy range from 100 to 500 eV and for both angles of incidence, the model calculation fits the experimental data very well.[16] The values of the parameter $\mu_t$ used in these fits are listed in Table I.

We now make a second approximation by supposing that all the multiple scattering is uniform in $2\theta$; this approximation will underestimate the multiple scattering since this flat contribution is most efficient in filling up the valleys in $I_1'(\vec{S})$. Using Eq. (8) to estimate $I_2'(\vec{S})$, Eq. (9) now becomes

$$I_T(\vec{S})=\left(1-\frac{2.76}{E^{1/2}\sin\phi}\right)\left(1-\frac{2.76}{E^{1/2}\sin\phi'}\right)\left(\frac{1}{1+\sin\phi/\sin\phi'}\right)$$

$$\times\left(\frac{\rho}{\mu_t}\right)\left[|f(\theta,E)|^2+\frac{\sigma_{el}^{b}}{2\pi}\sum_{n=2}^{\infty}\left(\frac{\rho\sigma_{el}^{f}}{\mu_t}\right)^{n-1}\right],\qquad(10)$$

where $\rho\sigma_{el}^{f}/\mu_t$ is now to be treated as an adjustable parameter.

In Figs. 7 and 8 fits for the best values of $\rho\sigma_{el}^{f}/\mu_t$
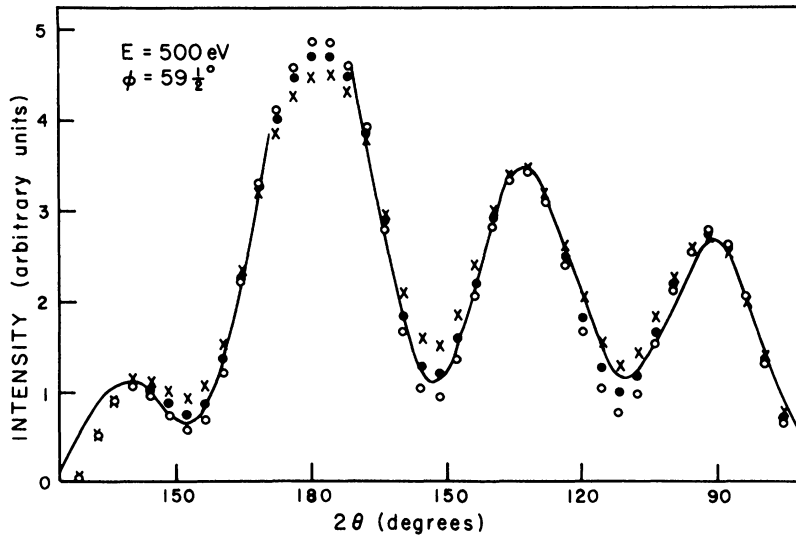


FIG. 6. Comparison of the model calculation results with the experimental data. Solid line is the observed data for $E = 500$ eV and $\phi = 59.9°$. The points are calculated from Eq. (9). Crosses: $\mu_t = 0.26$ Å$^{-1}$; filled circles: $\mu_t = 0.32$ Å$^{-1}$; open circles: $\mu_t = 0.42$ Å$^{-1}$.
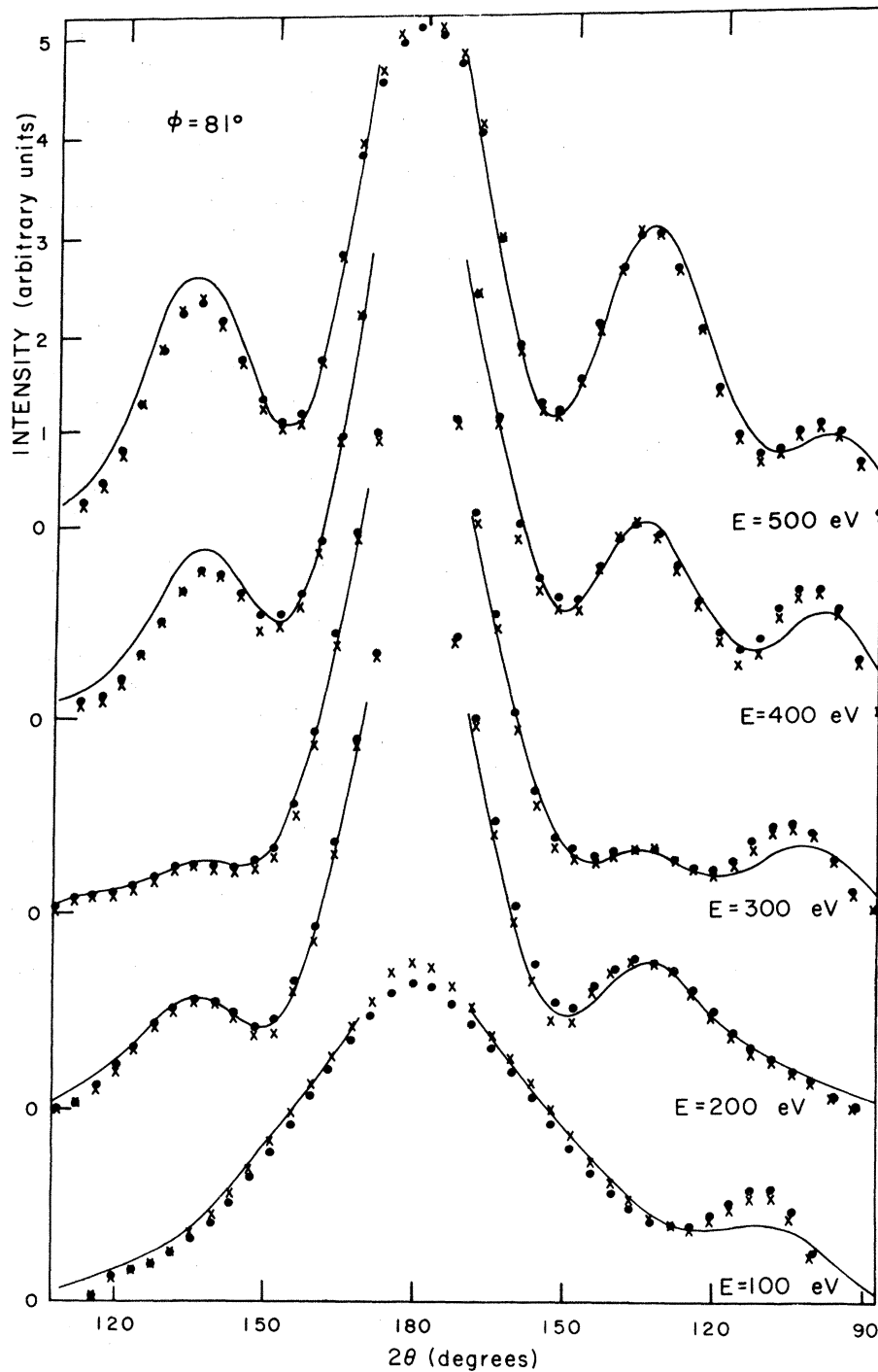
FIG. 7. Comparison of model calculation results with experimental data for several energies for $\phi = 81°$. The solid line is the experimental data. The dots are calculated from Eq. (9) using values of $\mu_t$ from Table I. The crosses are calculated from Eq. (10) using values of $\rho\sigma_{el}^f/\mu_t$ from Table I.

are shown as the crosses. These fits are as acceptable as those from the previous approximation. This emphasizes that the calculated angular dependence is not very sensitive to the detailed shape of the multiple scattering but rather depends mainly on the ratio $(\rho\sigma_{el}^f/\mu_t)$. Values of this parameter used for these fits are listed in Table I.

At first it may seem surprising that equally good fits to the observed angular dependence are obtained from the two different approximations leading to Eqs. (9) and (10). This is because the twice-scattered contribution is quite small and flat and because its shape is not greatly different from a sum of $|f(\theta, E)|^2$ and a constant. Therefore the
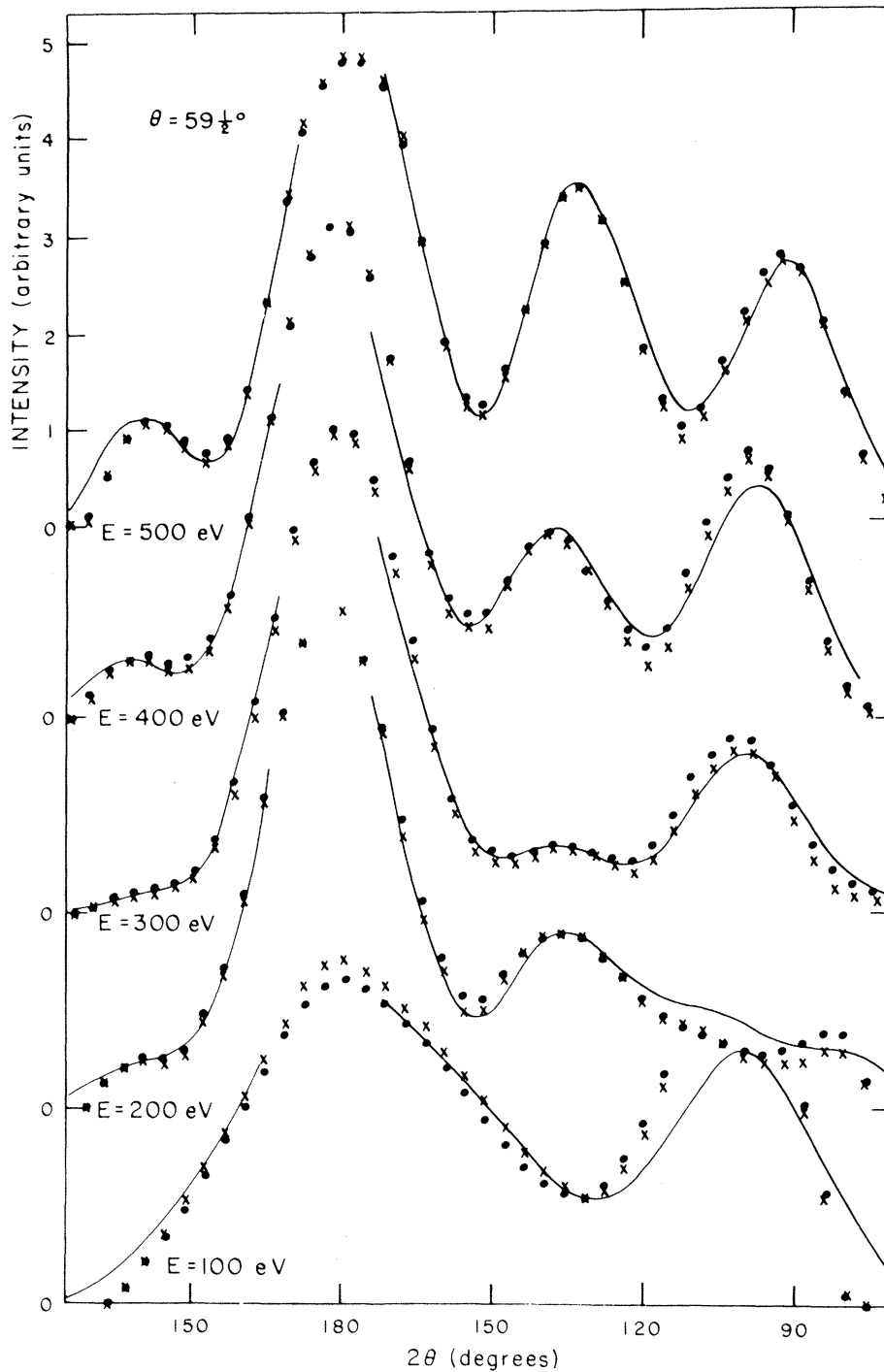
FIG. 8. Comparison of the model calculation results with experimental data for several energies for $\phi = 59.5°$. The solid line represents the data. The dots and crosses are calculated from Eqs. (9) and (10), respectively, using the values of the parameters determined for $\phi = 81°$.

fitting is sensitive to the values of the parameters $\mu_t$ and $\rho\sigma_{el}^{f}/\mu_t$, but not to which of the assumed shapes of $I_2'$ is used.

### V. DISCUSSION

This analysis has invoked multiple scattering and the attenuation due to inelastic processes to explain the differences between the scattering from the liquid and that from the free atom. Other causes of the differences could be considered, including the perturbation of the atom when it is put into the condensed phase, screening of the incident electrons by the conduction electrons, and interference due to the short-range order in the liquid.

TABLE I. Values of the parameters used in the fits shown in Figs. 7 and 8.

| Energy | $\mu_t(\text{Å}^{-1})$ | $\rho\sigma_{el}^{f}/\mu_t$ |
|--------|------------------------|------------------------------|
| 100 | 0.84 | 0.44 |
| 175 | 0.64 | 0.48 |
| 200 | 0.56 | 0.54 |
| 300 | 0.52 | 0.38 |
| 400 | 0.40 | 0.34 |
| 500 | 0.32 | 0.32 |



FIG. 9. Ratio of the singly scattered to total integrated intensities as a function of energy. Dots are calculated from Eq. (12) using $\sigma_{el}^{f}$ for the free atom and $\mu_t$ from Table I. Crosses are calculated using $\rho\sigma_{el}^{f}/\mu_t$ from Table I. The dashed line is calculated using free-atom cross sections. Error bars are for the dots only.

All of these must be present and affect the scattering to some extent. However, the success with which the observed scattering may be fitted by the model using reasonable values of the single parameter suggests that the dominant effects have been included. Had the other effects listed above been included in the model, an even smaller multiple-scattering contribution would have been required to fit the experimental data. The important and perhaps unexpected result is that the multiple scattering is relatively small. Therefore we shall assume that the model is essentially correct and now discuss some of its implications for the understanding of the diffraction of slow electrons from crystalline solids.

We first consider the multiply scattered contribution to the elastic intensity integrated over all back angles, which is given approximately by

$$\int_{\text{back angles}} I_T d\Omega = \left(\frac{\rho\sigma_{el}^{b}}{\mu_t}\right)\left[1 + \left(\frac{\rho\sigma_{el}^{f}}{\mu_t}\right) + \left(\frac{\rho\sigma_{el}^{f}}{\mu_t}\right)^2 + \cdots \right]$$

$$= \frac{\rho\sigma_{el}^{b}}{\mu_t}\left(1 - \frac{\rho\sigma_{el}^{f}}{\mu_t}\right)^{-1}. \qquad (11)$$

The ratio of the once-scattered to the total scattered intensities is then

$$\int I_1' d\Omega / \int I_T' d\Omega = 1 - \rho\sigma_{el}^{f}/\mu_t . \qquad (12)$$

Values of this ratio using the parameters given in Table I are plotted in Fig. 9 as a function of energy for each of the above approximations. Since these approximations tend to over- and underestimate the multiple scattering, it is concluded that about half of the observed intensity has been singly scattered and that this ratio is relatively independent of energy in the energy range of these experiments.

There is reason to suppose that for other liquids or thermally disordered solids the relative importance of the multiple scattering would be similar to that found here for Hg. The multiple scattering depends on the ratio $\rho\sigma_{el}/\mu_t = \sigma_{el}/(\sigma_{el}+\sigma_{in})$, where we have expressed the attenuation coefficient in terms of cross sections. For liquid Hg the parameters determined above give $\sigma_{el} \approx \sigma_{in}$. This same approximate equality holds also for the free
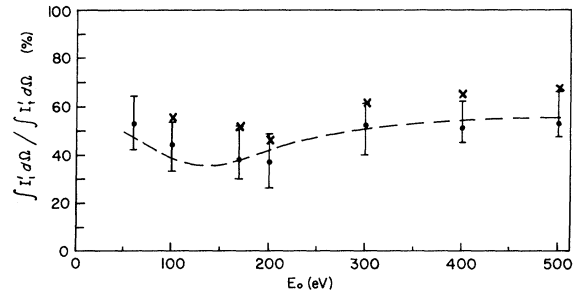
atom, as is illustrated in Fig. 10. In Fig. 9, the dotted line is the ratio from Eq. (12) evaluated using the free-atom cross sections. So for Hg and for the range of energies of interest here, the ratio of the elastic and inelastic total cross sections has not changed appreciably on condensation. (This can only be true in an average sense because of inelastic thresholds.) Furthermore, Lander [17] and Raether [18] have pointed out that the elastic and inelastic cross sections in this energy range are roughly equal for free atoms of many elements. Therefore, to the extent that for other elements this equality is unchanged going to the condensed phase, one expects roughly the same amount of multiple scattering.

The fact that singly scattered electrons constitute a large fraction of the observed elastically scattered electrons is the most significant result of the present work. This is contrary to those theoretical treatments of low-energy electron diffraction in
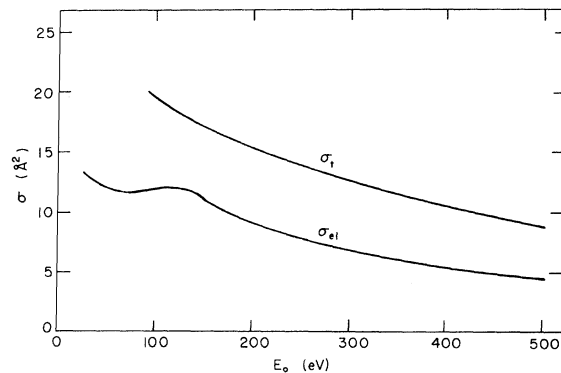


FIG. 10. Total elastic and total collision cross sections for Hg atoms. $\sigma_{el}$ is from Kessler (Ref. 11) and Arnot (Ref. 6). $\sigma_t$ is from Tate and Palmer (Ref. 6).

which inelastic effects are neglected and where multiple scattering is dominant. Because the singly scattered component is so large, it is reasonable that kinematic treatments including attenuation are often a reasonable first approximation; however, the present results indicate sufficient double and higher-order scattered amplitudes so their interference in the crystal can easily be responsible for the multiple-scattering secondary peaks and for anomalous Bragg intensities. Lander and Morrison[19] have previously discussed the role of inelastic processes in reducing dynamic effects. In fact, many of the present results could have been anticipated from their discussion. The present work supports the point of view of the recent "inelastic-collison model" of Duke and Tucker in which "inelastic loss mechanisms of an incident electron dominate the characteristics of its wave function inside the crystal."[1] This work also suggests that theories in which scattered amplitudes are followed through successive scatterings will converge rapidly and perhaps give a more transparent description of the diffraction than a complete self-consistent multiple-scattering theory or band-structure approach. A calculation of this type has been carried out by Gafner for Ni.[20] But whichever theoretical approach one uses for the diffraction problem, the present results emphasize the importance of taking proper account of the large inelastic scattering.

We now want to comment on the atomic scattering factor.

First, the present work supports the argument mentioned in the Introduction that $|f(\theta, E)|^2_{eff}$ is a useful approximation to $|f(\theta, E)|^2$ at back angles in the sense that the angular structure of the scattering observed from the disordered system is dominated by the single scattering and that multiple-scattering contributions add a background relatively independent of angle.

Second, both the observed similarity in the scattering from the liquid and from the free atom and the success of the model calculation indicate that for back angles $|f(\theta, E)|^2$ is essentially the same for atoms in the vapor and in the condensed phase. This might have been expected since the scattering for the diffraction vector $|\vec{S}| \gtrsim 5\text{Å}^{-1}$ should be most sensitive to variations in the potential over a spatial region the order of a few tenths of an Å. This is smaller than the Thomas-Fermi screening length and the radius of the ion core whose tightly bound electrons are not appreciably perturbed in the condensed phase. While this may simplify the theoretical interpretation of diffraction intensities by allowing use of free-atom scattering factors as a good approximation, it makes it unlikely that low-energy electron diffraction from high-$Z$ materials can yield much direct information about the perturbation of the valence electron structure by the surface. This would not be true of low-$Z$ materials where a large fraction of the electrons take part in the binding of the solid.

Finally, we consider inelastic processes. From Table I we conclude that $\sigma_{in} \approx \sigma_{el}$. To the extent that the elastic cross section is nearly geometrical in the condensed phase, the mean free path for inelastic processes is of the order of the interplanar spacing and $\mu_{in}$ is of the order of several tenths $\text{Å}^{-1}$. This agrees with other experimental estimates[21] and is of the order of magnitude needed in theoretical treatments[4] to give structure and widths in the energy profiles of the diffracted intensities in reasonable accord with experimental observations. It is this strong absorption of the elastic beam which is responsible for the rapidly diminishing contributions from successively higher-order multiple scatterings.

---

†Present address: Physik Dept., Technische Hochschule, München, Germany.

[1]See references and discussion by C. B. Duke and C. W. Tucker, Jr., Surface Sci. **15**, 231 (1969).

[2]For example, D. S. Bondreaux and V. Heine, Surface Sci. **8**, 426 (1967); J. B. Pendry (unpublished); R. M. Stern. J. J. Perry, and D. S. Bondreaux, Rev. Mod. Phys. **41**, 275 (1969).

[3]For example, E. G. McRae, J. Chem. Phys. **45**, 3258 (1966); K. Kambe, Z. Naturforsch. **22a**, 322 (1967).

[4]R. O. Jones and J. A. Strozier, Phys. Rev. Letters **22**, 1186 (1969); J. B. Pendry, J. Phys. C **2**, 2283 (1969); Y. H. Ohtsuki, J. Phys. Soc. Japan **24**, 1116 (1968).

[5]M. G. Lagally and M. B. Webb, Phys. Rev. Letters **21**, 1388 (1968); *The Structure and Chemistry of Solid Surfaces*, edited by G. A. Somorjai (Wiley, New York, 1969).

[6]For example, F. L. Arnot, Proc. Roy. Soc. (London) **A133**, 615 (1931); J. T. Tate and P. R. Palmer, Phys. Rev. **40**, 731 (1932); W. Eitel, K. Jost, and J. Kessler, Z. Physik **209**, 348 (1968); C. M. Yeates, thesis, Brigham Young University, Provo, Utah, 1967 (unpublished).

[7]W. Eckstein, Z. Physik **203**, 59 (1967).

[8]E. B. Jordan and R. B. Brode, Phys. Rev. **43**, 112 (1933).

[9]E. H. Sargent & Co.

[10]J. L. Schonfelder and P. J. Bunyan, Proc. Phys. Soc. (London) **85**, 455 (1965).

[11]J. Kessler and H. Lindner, Z. Physik **183**, 1 (1965).

[12]C. N. G. Wagner, H. Ocken, and M. J. Joshi, Z. Naturforsch. **20a**, 325 (1965).

[13]R. H. Ritchie, Phys. Rev. **106**, 874 (1957); E. A.

Stern and R. A. Ferrel, *ibid.* 120, 130 (1960); W. H. Weber and M. B. Webb, *ibid.* 177, 1103 (1969).

[14]E. G. Wilson and S. A. Rice, Phys. Rev. 145, 55 (1966).

[15]G. Holzwarth and H. J. Meister, *Tables of Asymmetry, Cross Section, and Related Functions for Mott Scattering of Electrons by Screened Gold and Mercury Nuclei* (München, 1964).

[16]The liquid and gas data used in these fits were taken at incident electron energies which may have been different by as much as 2% owing to voltmeter calibration. Interpolation of the gas data showed that, for such energy shifts, the changes in the gas data were smaller than the uncertainties in the gas data. To determine the importance of an inner potential correction, the liquid data were interpolated to an energy 11.6 eV below the gas data and refraction was included in the model calculation. The fits were essentially unchanged.

[17]J. J. Lander, Progr. Solid State Chem. 2, 26 (1965).

[18]H. Raether (private communication).

[19]J. J. Lander and J. Morrison, J. Appl. Phys. 34, 3517 (1963).

[20]G. Gafner, in *The Structure and Chemistry of Solid Surfaces*, edited by G. A. Somorjai (Wiley, New York, 1969).

[21]H. E. Farnsworth, Phys. Rev. 49, 605 (1936); P. W. Palmberg and T. N. Rhodin, J. Appl. Phys. 39, 2425 (1968); W. H. Weber and M. B. Webb, Phys. Rev. 177, 1103 (1969).

---

# Photoemission and Optical Studies of Cu-Ni Alloys. I. Cu-Rich Alloys*

D. H. Seib[†] and W. E. Spicer

*Stanford University, Stanford, California* 94305

(Received 24 October 1969; revised manuscript received 23 April 1970)

Photoemission and optical reflectivity measurements of Cu-rich Cu-Ni alloys are reported. The results for alloys of composition 87% Cu-13% Ni and 77% Cu-23% Ni give conclusive evidence that a virtual bound state rather than a rigid-band model is appropriate for describing the Ni $d$ states in Cu-Ni alloys. In these alloys, the Cu $d$ states are found to be little changed in energy position from the $d$ states in pure Cu. From the photoemission data, the Ni virtual bound state is found to be centered 0.95 eV below the Fermi energy, and the half-width at half-maximum of the state, due to $s$-$d$ interactions alone, is found to be $0.42 \pm 0.05$ eV. For the alloy compositions studied, it is also found that interactions among Ni states on different atoms give a significant contribution to the total width of the state. The behavior of alloy reflectivity data and optical parameters, which are deduced by a Kramers-Krönig analysis, is consistent with the alloy electronic structure obtained from the photoemission measurements.

## I. INTRODUCTION

The electronic structure and related properties of the alloys of copper with nickel have long been the subject of much theoretical and experimental interest. Cu-Ni alloys have often been taken to be the prototype of the many noble-metal–transition-metal systems, which involve the interaction of metals whose properties (at least near the Fermi surface) are determined by $s$-$p$ derived electron states and $d$-derived electron states, respectively. In addition, Cu-Ni alloys are ferromagnetic over more than one-half of the composition range and are (ideally) substitutional solid solutions over the entire composition range. These properties, and the fact that pure Cu and pure Ni are among the best understood of the noble and transition metals, have stimulated a great amount of work on the Cu-Ni alloy system.

Early magnetic moment[1] and optical data[2] for Cu-Ni alloys led Mott[3] to propose in 1935 the rigid- or common-band model of alloying behavior. The rigid-band model assumes that there is one electronic density-of-states function which is the same for Ni, Cu, and Cu-Ni alloys, with this density of states filled to an energy level determined by the electron-to-atom ratio. This model appears to still enjoy fairly wide acceptance.[4] However, many subsequent measurements have questioned the applicability of the rigid-band model to Cu-Ni alloys[5-14] and alternative models have been suggested.[15,16] In particular, it has been suggested[10-14] that a virtual-bound-state type of model, as developed by Friedel[17] and Anderson,[18] is appropriate for describing the electronic structure of Cu-rich Cu-Ni alloys.

These two different models – the rigid-band and the virtual-bound-state (VBS) models – predict quite different behavior for the density of states in Cu-Ni alloys. This is illustrated in Fig. 1. The drawing on the left-hand side of Fig. 1 illustrates schematically the optical density of states of pure